Airflow inside tunnel boring machine: A numerical study and an experimental verification

H.R. Nezarat[1], S.M.E. Jalali[1*] and M. Nazari[2]

1. Faculty of Mining, Petroleum & Geophysics Engineering, Shahrood University of Technology, Shahrood, Iran
2. Faculty of Mechanical & Mechatronics Engineering, Shahrood University of Technology, Shahrood, Iran

1. Introduction

The Tunnel Boring Machines (TBMs) have revolutionized the tunneling industry to make the underground space safer, healthier, and more economical. A TBM consists of a cutter head, a mainframe, and a backup system. Most of the mainframe in hard rock TBMs include shield body, main drive, erector, synchronized grouting system, transport system, and control cabin. When TBM is advancing, the heat and humidity generated at the mainframe cannot be discharged naturally, thus concentrate at the mainframe in the shape of fog. Most of the TBM crews stay and work in the mainframe area, so ventilation of this zone is very important. In some projects, emission of gases such as methane and combustible gas from the geological condition may be experienced in the mainframe. Thus the mainframe ventilation is very important for TBM equipment and crew.

The quality and quantity of airflow in TBM should be sufficient to dilute gases, remove dust, and control temperature.

In general, if the ventilation system is not taken into account in the TBM, hazards like silica dust, refractory ceramic or other mineral fibers and diesel particulate materials, toxic gases, fumes, vapors, and explosive and asphyxiant gases may be present. For example, an insufficient airflow and the explosion of methane gas injured four miners in Los Angles water transport tunnel, and similar accidents injured two workers and killed 9 in Higashimurayama (Japan) [1]. Another example is a TBM used at the Zagros water conveyance tunnel in the Kermanshah Province (Iran), where hydrogen sulfide, hydrogen cyanide, and methane gases were recorded with the concentration of methane gas above the explosion

✉ *Corresponding author: jalalisme@gmail.com (S.M.E. Jalali).*

level so that the tunnel operations were suspended for 4 months [2].

Numerical studies and modelings of airflow distribution have been developed for all underground mining and tunnel-construction activities. Most of the numerical simulation studies on the tunnel and underground space ventilation are in airflow distribution, gas emission, dust dispersion, and Diesel Particulate Matter (DPM).

Recently, airflow modeling with Computational Fluid Dynamic (CFD) has been developed in underground mines and tunnels. Wala *et al.* studied airflow patterns around the workspace of continuous miners with different boring patterns [3]. Aminossadati and Hooman modeled a 2D model in order to evaluate the effect of brattice length on the airflow velocity [4]. Zheng and Tien used Fluent and Gambit to evaluate the airflow pattern and DPM concentration in underground mines [5]. Taylor *et al.* investigated the impact of the setback distance on airflow and methane distribution [6]. Diego *et al.* calculated air losses in circular tunnels by both the traditional and CFD methods [7]. A computational study was carried out to investigate the airflow behavior and methane distribution in the room and pillar underground coal mine [8]. Xu *et al.* used the trace gas technology and CFD to simulate airflow inside the mines [9].

Gas and methane concentration is another attractive research topic. Parra *et al.* were directed to explore gas emission in the underground coal mines. They modeled three different ventilation systems including blowing, exhaust, and mixed ventilation using CFD [10]. Rodriguez and Lombardia calculated methane concentration and quantified air flow in TBM according to a mathematical equation [11]. Torno *et al.* solved numerical simulation for the dilution behavior of blasting gases, especially carbon monoxide (CO) concentration [12]. Kurnia *et al.* numerically investigated diesel exhaust gas as a species mixture in an underground mine [13]. Zhou *et al.* modeled methane distribution at continuous miner face with various curtain set-back distances [14]. Widiatmojo *et al.* predicted sulfur hexafluoride (SF6) gas dispersion in coal mine ventilation system by CFD modeling and experimental verification [15].

There have been many relevant researchers aiming to improve the efficiency of dust and DPM control. Qiao *et al.* monitored concentration of Particulate Matter (PM) in the subway tunnel [16]. Torano *et al.* used CFD to predict airflow and dust dispersion in a mechanized underground coal mine [17]. Kurnia *et al.* validated a 3D CFD model utilizing the Eulerian-Lagrangian approach to track the dispersion of dust particle [18]. Hu *et al.* studied coal dust particle behavior after blasting in a roadway [19]. Thiruvengadam *et al.* simulated DPM by CFD and comparison between the particle and species model [20]. Xia *et al.* used CFD to simulate dust suppression for open-type TBM [21]. Zheng *et al.* revealed the effect of single dead-end entry inclination on DPM plume dispersion by CFD methods [22]. Yueze *et al.* predicted air flow methane and coal dust dispersion in room and pillar mining face using the CFD approach [23].

In summary, the numerical study of airflow has mainly been concentrated on underground mines and road tunnels. Ventilation during the construction of long tunnels, especially the ventilation of TBMs has received less attention. The two specific objectives of this paper are first to study the airflow pattern in the TBM ventilation system, and secondly, to decreased dead zones to solve safety and health problems. Experimental measurements were carried out on the Chamshir tunnel to validate the results of a 3D numerical model. The results obtained illustrate the airflow pattern of a TBM ventilation system. The present study can help the engineers to design an effective ventilation system for TBMs.

The layout of this paper is as what follows. Firstly, the physics and geometry of the case study are introduced. The governing principles and theories comprise turbulence conservation of mass, momentum, and energy equations. The mesh generation and mesh independence principles were then discussed. Boundary conditions were set by the experimental data. The model was then solved numerically using the commercial computational fluid dynamics solver, Ansys CFX 18.1. The results obtained identified the dead zones in the location with low airflow velocity. Three different scenarios were investigated with respect to jet fan characteristics. Air velocity was increased by 20%, 40%, and 60% in the inlet, and the variations in air velocity were analyzed. Finally, conclusions were drawn and extensions of the work were highlighted.

2. Methodology

In this work, we modeled the TBM ventilation system using the CFD method to obtain an understanding of the airflow behavior in a TBM. The experimental measurements were carried out

on the Chamshir Tunnel to validate the results of a 3D numerical model.

2.1. Physics of problem

The considered modeling area was the whole space of TBM in the Chamshir tunnel. The Chamshir water transport tunnel is located in the south of Iran. This tunnel was constructed using a single-shield TBM and had a final diameter of 4.6 m. Three axial-type blowing fans were connected serially in the portal of the Chamshir tunnel and fresh air was sent with flexible ducting forming the tunnel portal to the end of backup system in a 1400 m length. In order to deliver fresh air to the TBM mainframe area, a blowing jet fan (55 KW) with a hot dip galvanized duct was installed in gantry 2, which could be observed in Figure 1. The wye tee (pant) divided the airflow duct between two parallel legs as inlets 1 and 2. The setback distance (distance of the ventilation duct from the shield space) in the inlets 1 and 2 was 16 m and 19 m, respectively. Figure 1 represents the exhaust jet fan with a 15 KW power in gantry 4 sucked pollutants, which was produced by a locomotive and send it to the end of the backup system. Due to the geometric complexities of the problem, simplifications were made in the machine geometry according to Figure 1. These simplifications were done in a manner that did not affect the main airflow field and accuracy of the modeling results. For example, pipe for oil, water, and compressed air were not included in the computational model. To this end, the 3D model of machine geometry was developed by SpaceClaim 18.1.

2.2. Governing equations

The 3D modeled airflow was considered as an incompressible, viscous, Newtonian, steady state, and turbulent flow. In addition, the tunnel walls were covered by segments and were sealed with gasket, although it was assumed that the tunnel walls were insulated and there existed isothermal ventilation. The radiation heat transfer and the effect of tunnel slope on ventilation were neglected. Based on the assumptions made, the airflow in the whole workspace of the studied TBM could be solved by the Reynolds-Averaged Navier-Stokes (RANS) equations [24].

2.3. Boundary conditions

The CFD model used three types of boundary conditions: wall, inlet, and outlet. There were four inlets and three outlets in TBM, as shown in Figure 1. The blowing air duct outlets (inlets 1 and 2), exhaust air duct inlet (inlet 3), portal blowing duct outlet (inlet 4), blowing air duct inlet (outlet 2), and exhaust air duct inlet (outlet 2) had a boundary type of VELOCITY_INLET. The roadway rear outflow (outlet 1) had a boundary type of PRESSURE_OUTLET. To define the boundary conditions, the airflow velocity sampling was performed using the multi-point sampling method in the ductwork outlet. The British Standard Institute (BSI) have recommended five sampling points, which are to be located as shown in Figure 2a [25]. In multi-point sampling, the measured cross-section was divided into 4 equal areas. The centers of the four areas and the general center, totally 5 points, were selected as the sampling points. This whole procedure was repeated for three times for each individual to reduce error and variation. A mini-vane anemometer, model EM-9000, was used to measure the air velocity (Figure 2b). A mini-vane anemometer is an instrument that rotates at a speed directly proportional to the air speed and measures the air velocity. The arithmetic mean of the points was considered as an average air velocity [26]. Table 1 shows the statistical parameter of the inlet and outlet velocity-based boundary condition. The outlet 1 boundary condition was set to the atmospheric pressure. The boundary condition of wall surfaces was considered as no-slip wall.

2.4. Mesh generation in computational domain

The computational grid was generated by the commercial software ANSYS ICEM CFD. To have a good sensitivity, high-density elements were inserted near the wall and the bounding wall regions. The first grid (near the walls) was located inside the viscous sub-layer by satisfying $y^+ < 3$. Both the hexahedral and tetrahedral meshes were generated inside the computational domain. Five different numbers of grids, i.e. 27×10^6, 36×10^6, 49×10^6, 52×10^6, and 57×10^6, were implemented and compared in terms of local velocity to ensure a mesh-independent solution. According to Figure 3, comparison of the number of mesh elements with air velocity in station number 3 shows that the variations in air velocity in this station between a 49 million element and a 52 million element is less than 1%, while the difference between a 36 million element network and a 49 million element exceeds 20%. This implies that in this step, 49 million element cells are sufficient for the present modeling. During the mesh generation, the mesh quality as aspect ratio, skewness, and orthogonal quality were monitored

and maintained to have a good meshing. Table 2 shows the statistical parameters of mesh quality in a 49 million element model in terms of the aspect ratio, skewness, and orthogonal quality.

Therefore, a mesh of around 49 million with a quality of 0.74, considered to be acceptable for the CFD method, was selected [27].
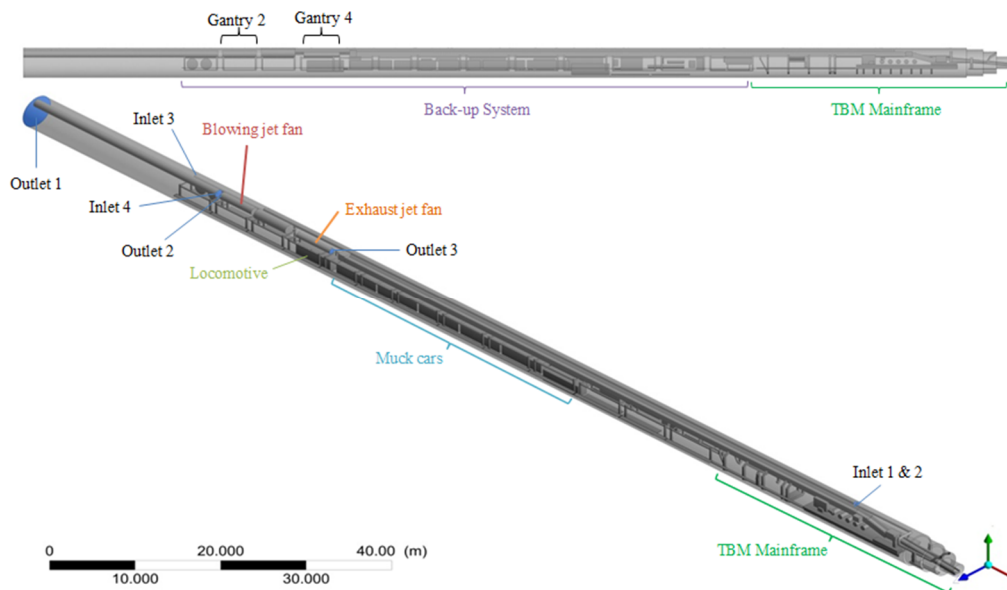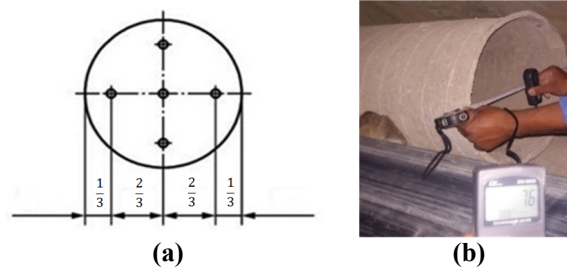

Figure 1. TBM geometry model.

| (a) | (b) |

Figure 2a. Location of sampling points in multi-point method. B. Air velocity sampling by mini-vane anemometer.

Table 1. Statistical parameters of inlet and outlet boundary condition.

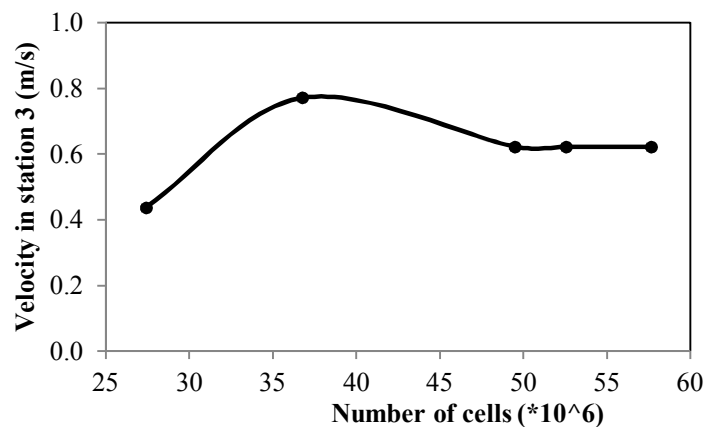| Parameter	Inlet 1	Inlet 2	Inlet 3	Inlet 4	Outlet 2	Outlet 3
Average air velocity (m/s)	7.9	5.6	18	10.04	2.73	7.7
Standard deviation	0.07	0.08	0.12	0.1	0.09	0.08

Figure 3. Mesh generation with different mesh sizes and local velocities at station 3.

Table 2. Mesh generation statistical parameter in a 49 million element model.

Parameter	Element quality	Aspect ratio	Skewness	Orthogonal quality
Average	0.74	0.75	0.25	2.56
Standard deviation	0.2	0.15	0.15	5.92

2.5. Solution strategy

Different authors such as Parra *et al*., 2006, Torno et al., 2013, Kurnia *et al*., 2014, Yueze *et al*., 2015, and Zhou *et al*., 2017 have found that there is a positive correlation between the measured values and those estimated by standard K–ε turbulence modeling in underground mines and tunnels [10, 12, 13, 23, 28]. Therefore, in this work, we used the standard K–ε model. The governing equations were integrated over each control volume. To complete the discretization of the advection term, the high-resolution scheme was computed [24]. Root Means Square (RMS) $< 10^{-4}$ was considered as the convergence criterion of mass and momentum equations. A computer with 24 processors and 60 GB RAM was used for convergence purposes, where 3000 iterations were calculated in about 98 h. To evaluate convergence, mass and momentum imbalance were considered below 1% in different directions. In addition, air velocity was monitored until it no longer changed with more iteration. When convergence was assured, the curve of the variations in air velocity in the lateral sections of the studied TBM was developed in order to assess the airflow distribution.

3. Results and discussion

The numerical simulations were carried out for a typical condition found in single-shield TBM. One of the key factors that determine the performance of ventilation system is the airflow velocity inside TBM. Looking into the airflow velocity at various cross-sections in the mainframe of TBM, as displayed in Figure 4, it was found that a high air velocity flowed at the bottom of section 11 and gradually decreased toward section 1. Interestingly, the fresh air was supplied from the intake ventilation ducts and flew forward until it met the shield space, and air changed the flow direction and went along the segment feeder.
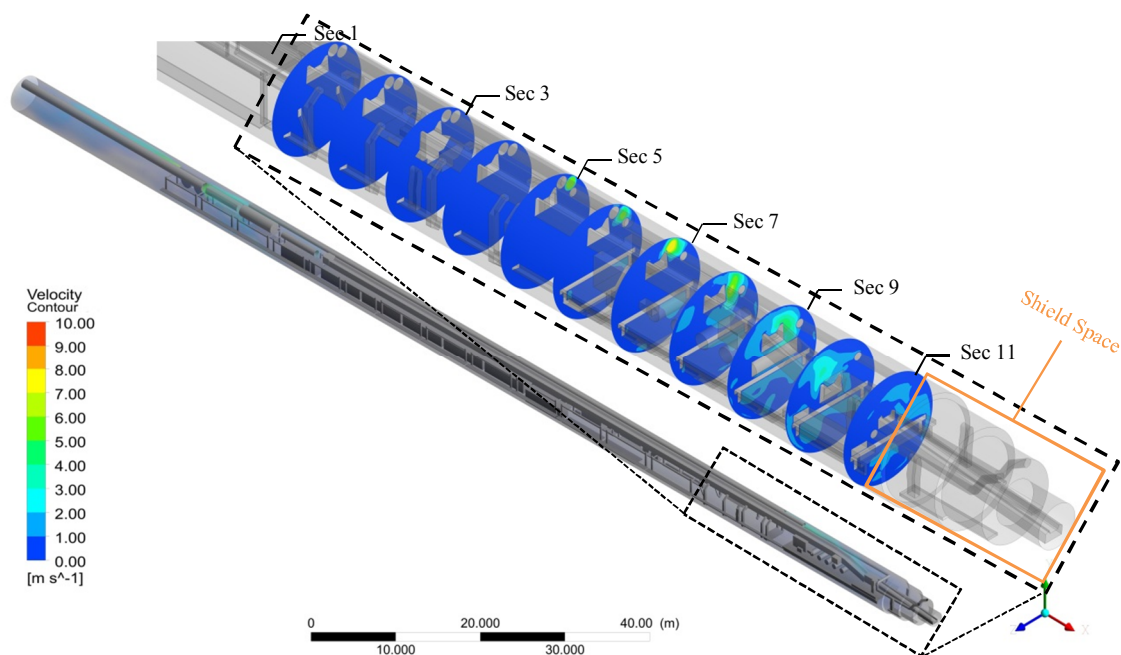

Figure 4. Air velocity contour in the mainframe of TBM.

The TBM crews were present in the bridge and worked in the top left corner of TBM. Thus the airflow velocity should be sufficient in this area. According to the international tunneling and underground space association guidelines for good occupational health and safety practice in tunnel construction, the quantity of air supplied or extracted from the face should be such that the average flow in the full cross-section of the tunnel or shaft should be between 0.3 m/s and 2 m/s at all times [29]. An area with average air velocity less than 0.3 m/s is deemed as the ''dead zone''. In

this zone, dangerous gases, dust, and other pollutants may be accumulated due to the low air velocity. The air velocity contour of the tunnel based on dead zone of each cross-section was obtained, as shown in Figure 5. The results obtained show that the dead zones are present in sections 1 to 7 in the crew pathway and staying places. According to the current situation in boundary condition, the modeling results show that the dead zones are in 59.6% volume of TBM, and airflow is not sufficient for the ventilation of TBM. This airflow quantity is low and dead zone is present in the region of 20 m away from shield space (shown as dash line area in Figure 5k).

a) Dead Zone in cross-section no. 1

b) Dead Zone in cross-section no. 2

c) Dead Zone in cross-section no. 3c

d) Dead Zone in cross-section no. 4

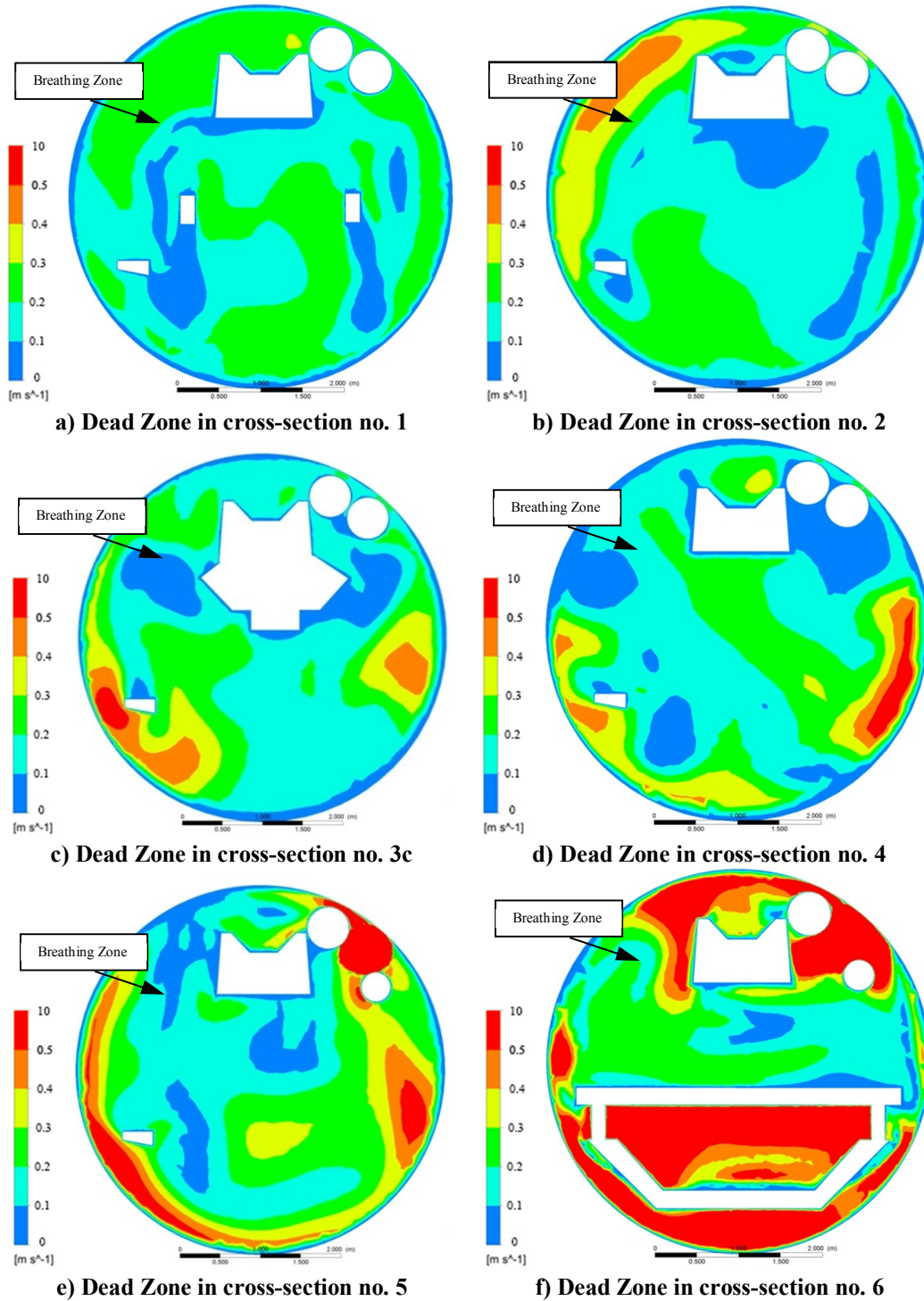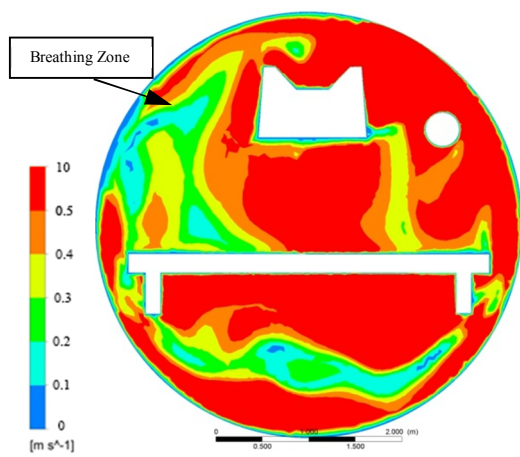**e) Dead Zone in cross-section no. 5**

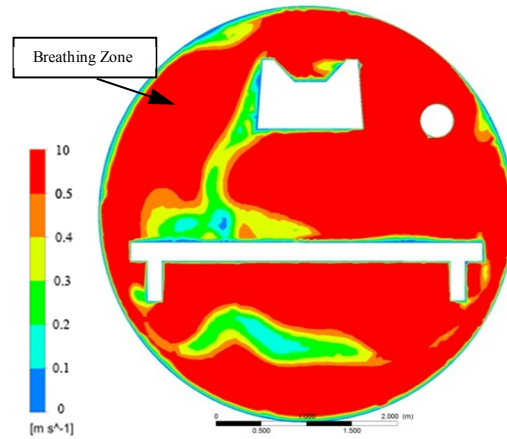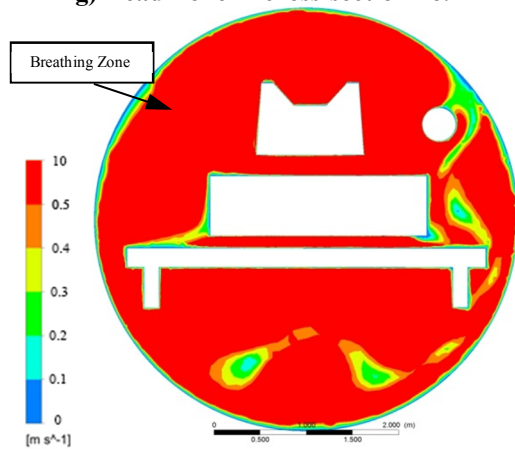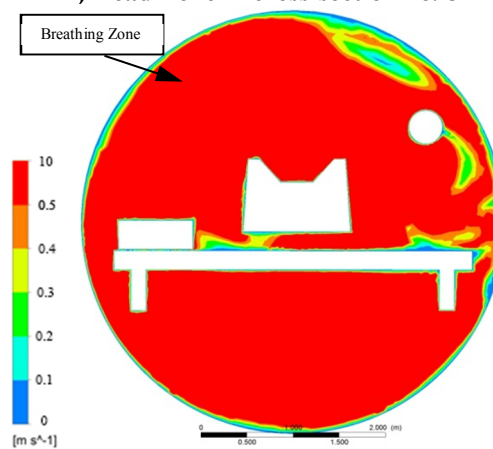**f) Dead Zone in cross-section no. 6**

Figure 5. Velocity contour and dead zones at TBM.
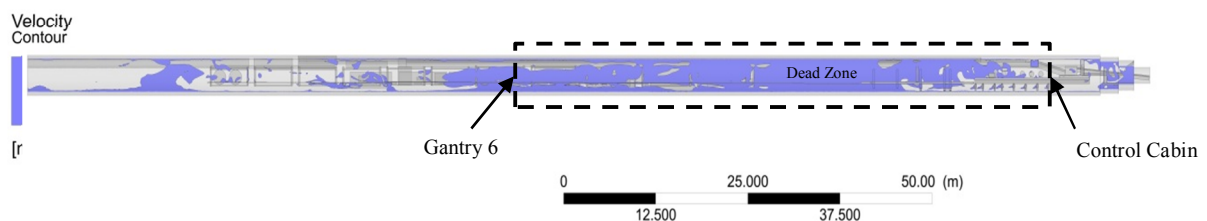
628

g) Dead Zone in cross-section no. 7

h) Dead Zone in cross-section no. 8

i) Dead Zone in cross-section no. 9

j) Dead Zone in cross-section no. 10

k) Dead Zone in longitudinal crew pathway section
Figure 5. Continued.

3.1. Verification of results

In order to validate the CFD model, airflow velocities were measured using a vane anemometer, model EM-9000, at a point 170 cm high from the bridge. The measurements were done in 5 stations. The measurements were also repeated for 5 times at different points to have 5 acceptable samples. In the measurement where airflow velocity deviated by $\geq 10\%$, the sampling was cancelled and was not considered in calculations. After computing the average and standard deviation of air velocity in each station, the experimental results were compared with the values derived from the numerical modeling. Figure 6 show both the numerical and experimental results including the related

confidence intervals (error bars) for various stations. It can be seen that the simulated velocity in all cases is in good agreement with the experimental results with no more than 2% error. The difference is larger in case S11, where velocity is < 0.5 m/s. This is because the mini-vane anemometer used in the experiment is limited in range at a velocity equivalent to a velocity less than 0.5 m/s.

According to Figure 6, in all stations, the variation in air velocity agrees between the experimental and modeled values, where the modeled results lie inside the confidence interval of the experimental data. The coefficient of determination (R^2) was used to compare the values derived from modeling and experimental measurements. This

coefficient ranges from zero to one. A coefficient of determination > 0.5 can be accepted for modeling [30, 31]. The computation results in Figure 7 show that the coefficient of determination is 0.9467. This means that there is a very high and positive correlation between the modeling velocities and the experimental velocities. This implies the high accuracy of modeling. The reason for some slight differences between results may be traced in the steady-state assumption of flows as well as simplifications made on the geometry. The effects of air humidity and temperature were neglected due to negligible changes in the measurement time. Generally, the comparison indicated that the CFD models were valid and could be used to conduct airflow modeling.
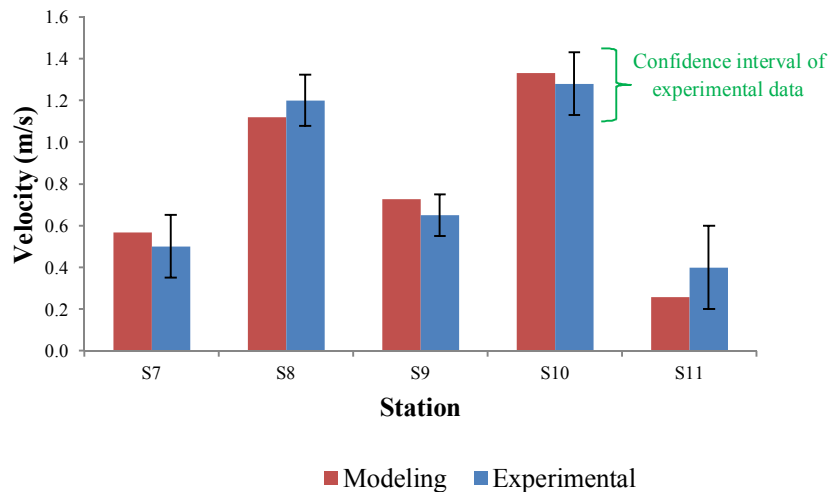

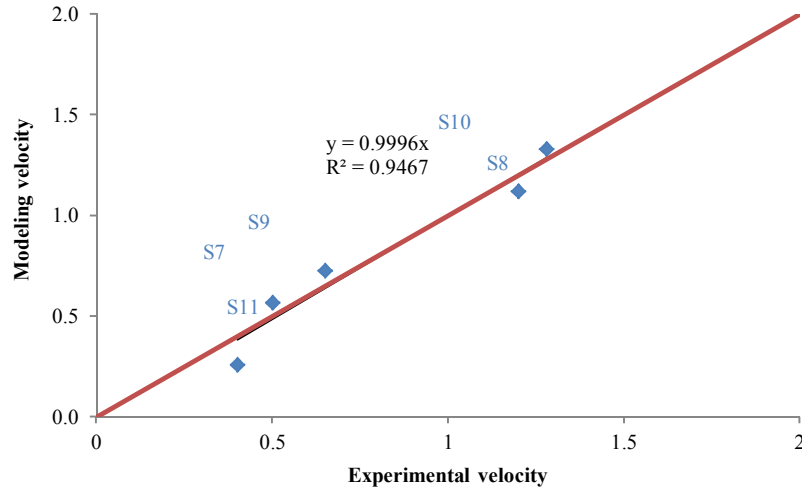**Figure 6. Comparing experimental air velocity with modeling results in different stations.**

Figure 7. Regression graph between experimental and modeling airflow velocity.

3.2. Sensitivity analysis

Several relevant scenarios were studied to decrease the number of dead zones and optimized relative airflow velocity. The measurement airflow velocity is used as a basic model for the benchmark in sensitivity analysis. To this end, air velocity was increased by 20%, 40%, and 60% in blowing jet fan. This scenario is available by speed-up jet fan ventilation system or installing other high capacity jet fans. After the simulation details, boundary conditions and dead zone volumes are listed in Table 3. The results show that as air mass flow increases by 20%, 40%, and 60%, the size of dead zones decreases by 1.79%, 4.36%, and 5.21%, respectively. It can be seen in Figure 8 that air mass flow has a good effect on the reduction of dead zones in the personal breathing zone. Scenarios planning at section 5 improve air velocity in the breathing zone 21.18%, 37.07%, and 65.25%, respectively.

Table 3. Influence of increasing air velocity inlets on dead zone volume.

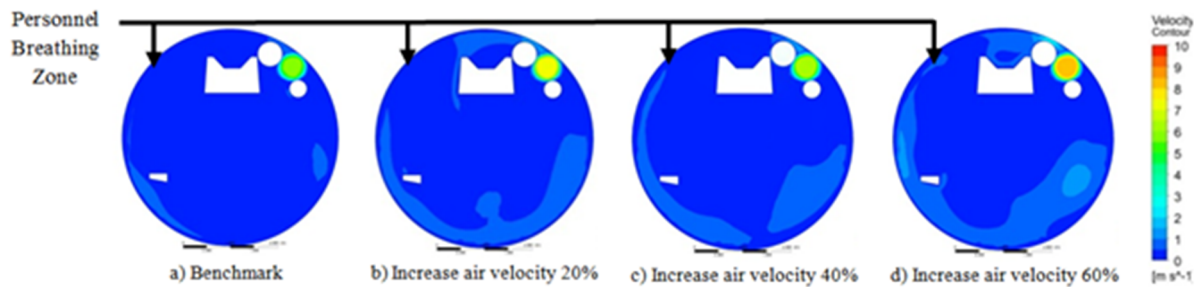|	Velocity Inlet 1 (m/s)	Velocity Inlet 2 (m/s)	Dead Zone Volume (m^3)	Dead Zone decreasing ratio (%)
Benchmark	7.9	5.6	1268.59	-
Scenarios 1	8.79	6.24	1245.78	-1.79
Scenarios 2	10.25	7.27	1213.29	-4.36
Scenarios 3	11.69	8.33	1202.45	-5.21

Figure 8. Influence of increasing air inlets on velocity contours at Section 5.

4. Conclusions

The air flow distribution in single-shield TBM was numerically investigated by utilizing the CFD approach. Field measurements carried out in the Chamshir tunnel have allowed validating a numerical model. Coefficient of determination in experimental and modeling results was calculated to be 0.9467. Based on the simulation results and analysis of airflow distribution, dead zones are present in sections 1 to 7 in crew pathway and staying place. Dead zone volume in benchmark is about 59.6% of the total space of the machine. Effect of increasing air mass flow rate on TBM ventilation was examined with regards to the personal safety. In summary, if blowing jet fan operates at maximum, the flow rate can decrease 5.21% dead zone volume and improve 65.25% airflow velocity in the breathing zone at the mainframe of TBM.

5. Recommendations

In this paper, the ventilation system in single-shield TBM was discussed. However, there are a great many scientific problems that require to be further researched such as the locomotive and TBM movement as dynamic mesh and the influence of diesel particulate matter and gas emission from the rock on the induced airflow, and the interaction of the pollutants gas with each other on the induced airflow, and others at TBMs. It is the hope of the authors that additional researchers will devote themselves to the correlation research works.

References

[1]. Deer, D. (1981). Adverse geology and TBM tunneling problems, Proc, 5th rapid excavation and tunneling conference, San Francisco, California. pp. 574-585.

[2]. Satari, G., Ajodani, S. and Bathaie, H. (2011). Mechanized tunneling in water and gas crisis, case study of Zagros tunnel, Proc, First asian and 9th iranian tunneling symposium. Tehran.

[3]. Wala, A., Jacob, J., Brown, J. and Huang, G. (2003). New approaches to mine-face ventilation. Mining Engineering. 55 (3): 25-30.

[4]. Aminossadati, S. and Hooman, K. (2008). Numerical Simulation of ventilation Air flow in underground mine working, Proc, 12th U.S./North American Mine Ventilation Symposium. Nevada: The University of Nevada, Reno. pp. 253-259.

[5]. Zheng, Y. and Tien, J. (2008). DPM dispersion study using CFD for underground metal/non-metal mines, Proc, 12th U.S./North American Mine Ventilation Symposium. Nevada: The University of Nevada, Reno. pp. 487-493.

[6]. Taylor, C., Chilton, J. and Goodman, G. (2010). Guidelines for the control and monitoring of methane gas on continuous mining operations. Pittsburgh: Department of Health and Human Services. doi:10.26616/nioshpub2010141.

[7]. Diego, I., Torno, S., Torano, J., Menendez, M. and Gent, M. (2011). A practical use of CFD for ventilation of underground works. Tunnelling and Underground Space Technology. 26 (1): 189-200.

[8]. Sasmito, A.P., Birgersson, E., Ly, H.C. and Mujumdar, A.S. (2013). Some approaches to improve ventilation system in underground coal mines

environment – A computational fluid dynamic study. Tunnelling and Underground Space Technology. 34: 82-95.

[9]. Xu, G., Luxbacher, K.D., Ragab, S. and Schafrik, S. (2013). Development of a remote analysis method for underground ventilation systems using tracer gas and CFD in a simplified laboratory apparatus. Tunnelling and Underground Space Technology. 33: 1-11.

[10]. Parra, M.T., Villafruela, J.M., Castro, F. and Méndez, C. (2006). Numerical and experimental analysis of different ventilation systems in deep mines. Building and Environment. 41 (2): 87-93.

[11]. Rodríguez, R. and Lombardía, C. (2010). Analysis of methane emissions in a tunnel excavated through Carboniferous strata based on underground coal mining experience. Tunnelling and Underground Space Technology. 25 (4): 456-468.

[12]. Torno, S., Toraño, J., Ulecia, M. and Allende, C. (2013). Conventional and numerical models of blasting gas behaviour in auxiliary ventilation of mining headings. Tunnelling and Underground Space Technology. 34: 73-81.

[13]. Kurnia, J.C., Sasmito, A.P., Wong, W.Y. and Mujumdar, A.S. (2014). Prediction and innovative control strategies for oxygen and hazardous gases from diesel emission in underground mines. Science of The Total Environment. 481: 317-334.

[14]. Zhou, L., Pritchard, C. and Zheng, Y. (2015). CFD modeling of methane distribution at a continuous miner face with various curtain setback distances. International Journal of Mining Science and Technology. 25 (4): 635-640.

[15]. Widiatmojo, A., Sasaki, K., Widodo, N.P., Sugai, Y., Sahzabi, A.Y. and Nguele, R. (2016). Predicting gas dispersion in large scale underground ventilation: A particle tracking approach. Building and Environment. 95: 171-181.

[16]. Qiao, T., Xiu, G., Zheng, Y., Yang, J. and Wang, L. (2015). Characterization of PM and Microclimate in a Shanghai Subway Tunnel, China. Procedia Engineering. 102: 1226-1232.

[17]. Toraño, J., Torno, S., Menéndez, M. and Gent, M. (2011). Auxiliary ventilation in mining roadways driven with roadheaders: Validated CFD modelling of dust behaviour. Tunnelling and Underground Space Technology. 26 (1): 201-210.

[18]. Kurnia, J.C., Sasmito, A.P., Hassani, F.P. and Mujumdar, A.S. (2015). Introduction and evaluation of a novel hybrid brattice for improved dust control in underground mining faces: A computational study. International Journal of Mining Science and Technology. 25 (4): 537-543.

[19]. Hu, S., Feng, G., Ren, X., Xu, G., Chang, P., Wang, Z., Zhang, Y., Li, Z. and Gao, Q. (2016). Numerical study of gas–solid two-phase flow in a coal roadway after blasting. Advanced Powder Technology. 27 (4): 1607-1617.

[20]. Thiruvengadam, M., Zheng, Y. and Tien, J.C. (2016). DPM simulation in an underground entry: Comparison between particle and species models. International Journal of Mining Science and Technology. 26 (3): 487-494.

[21]. Xia, Y., Yang, D., Hu, C., Wu, C. and Han, J. (2016). Numerical simulation of ventilation and dust suppression system for open-type TBM tunneling work area. Tunnelling and Underground Space Technology. 56: 70-78.

[22]. Zheng, Y., Lan, H., Thiruvengadam, M., Tien, J.C. and Li, Y. (2017). Effect of single dead end entry inclination on DPM plume dispersion. International Journal of Mining Science and Technology. 27 (3): 401-406.

[23]. Yueze, L., Akhtar, S., Sasmito, A.P. and Kurnia, J.C. (2017). Prediction of air flow, methane, and coal dust dispersion in a room and pillar mining face. International Journal of Mining Science and Technology. 27 (4): 657-662.

[24]. ANSYS. (2006). Ansys CFX- Solver theory guide. Canonsburg: ANSYS Inc.

[25]. BSI. (1983). Method for measurement of particulate emission including grit and dust (simplified method).

[26]. Goodfellow, H. and Tahti, E. (2001). Industrial Ventilation Design Guidebook. London: Academic Press. doi:10.1016/b978-012289676-7/50003-5

[27]. ANSYS. (2010). ANSYS Meshing User Guide. Canonsburg: ANSYS Inc.

[28]. Zhou, L., Pritchard, C. and Zheng, Y. (2015). CFD modeling of methane distribution at a continuous miner face with various curtain setback distances. International Journal of Mining Science and Technology. 25 (4): 635-640.

[29]. ITA, W.G. (2008). Guidelines for good occupational health and safety practice in tunnel construction. Avignon: International tunneling and underground space association.

[30]. Legates, D.R. and McCabe, G.J. (1999). Evaluating the use of "goodness-of-fit" Measures in hydrologic and hydroclimatic model validation. Water Resources Research. 35 (1): 233-241.

[31]. Moriasi, D.N., Arnold, J.G., Van Liew, M.W., Bingner, R.L., Harmel, R.D. and Veith, T.L. (2007). Model Evaluation Guidelines for Systematic Quantification of Accuracy in Watershed Simulations. Transactions of the ASABE. 50 (3): 885-900.

جریان هوا در ماشین حفاری تمام مقطع: مطالعه عددی و اعتبارسنجی میدانی

حمیدرضا نظارت¹، سید محمد اسماعیل جلالی¹* و محسن نظری²

۱- دانشکده مهندسی معدن، نفت و ژئوفیزیک، دانشگاه صنعتی شاهرود، ایران

۲- دانشکده مهندسی مکانیک و مکاترونیک، دانشگاه صنعتی شاهرود، ایران

* نویسنده مسئول مکاتبات: jalalisme@gmail.com

چکیده:

بررسی توزیع جریان هوا در داخل ماشین حفاری تمام مقطع تونل می‌تواند یک محیط ایمن برای پرسنل و تجهیزات ایجاد کند. کمیت و کیفیت هـوا در سـامانه تهویه باید کافی باشد تا گازها ترقیق شود و گردوغبار از بین برود. در این پژوهش، توزیع جریان هوا در ماشـین حفـاری تمـام مقطـع تـک سـپره بـا اسـتفاده از دینامیک سیالات محاسباتی مطالعه شده است. از روش حجم محدود مبتنی بر المان برای شبیه‌سازی سیال در هندسه پیچیده ماشین حفاری استفاده شده است. به منظور اعتبارسنجی نتایج مدل‌سازی عددی، سرعت هوا در مقاطع مختلف ماشین حفاری در تونل چم‌شیر اندازه‌گیری شده است. تونل انتقال آب چـم‌شـیر بـا طول ۷۰۵۰ متر و قطر نهایی ۴/۶ متر در جنوب ایران واقع شده است. نتایج مدل‌سازی نشان داد در شرایط حاضر در ۵۹/۶٪ از حجم ماشین حفاری جریان هوای کافی وجود ندارد؛ به عبارت دیگر، از اتاق کنترل تا پایان گنتری شماره ۶ در قسمت پشتیبان ماشین را منطقه مرده در برگرفته است. چندین راهبرد عملی برای حذف منطقه مرده و بهینه‌سازی سرعت جریان هوا با بهره‌گیری از بادبزن با ظرفیت بالاتر در سامانه تهویه مطالعه شده اسـت. نتـایج ایـن پـژوهش نشـان داد بـا افزایش شدت جریان هوا حجم منطقه مرده می‌تواند به میزان ۲۱/۵٪ کاهش یابد.

کلمات کلیدی: جریان هوا، ماشین حفاری تمام مقطع، تهویه، دینامیک سیالات محاسباتی، مدل‌سازی.